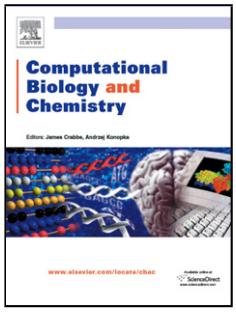

Title: Label-free optical biosensor for target detection based on simulation-assisted catalyzed hairpin assembly

Authors: Yingying Zhang, Luhui Wang, Yanan Wang, Yafei Dong

PII: S1476-9271(18)30794-1
DOI: https://doi.org/10.1016/j.compbiolchem.2018.11.030
Reference: CBAC 6974

To appear in: *Computational Biology and Chemistry*

Received date: 27 October 2018
Revised date: 26 November 2018
Accepted date: 30 November 2018

Please cite this article as: Zhang Y, Wang L, Wang Y, Dong Y, Label-free optical biosensor for target detection based on simulation-assisted catalyzed hairpin assembly, *Computational Biology and Chemistry* (2018), https://doi.org/10.1016/j.compbiolchem.2018.11.030

Label-free optical biosensor for target detection based on simulation-assisted catalyzed hairpin assembly

Yingying Zhang [a], Luhui Wang [b], Yanan Wang [a] and Yafei Dong [b,*]

[a] School of Computer Science, Shaanxi Normal University, Xi'an 710119, China

[b] College of Life Sciences, Shaanxi Normal University, Xi'an 710119, China

* Correspondence: dongyf@snnu.edu.cn

Graphical Abstract

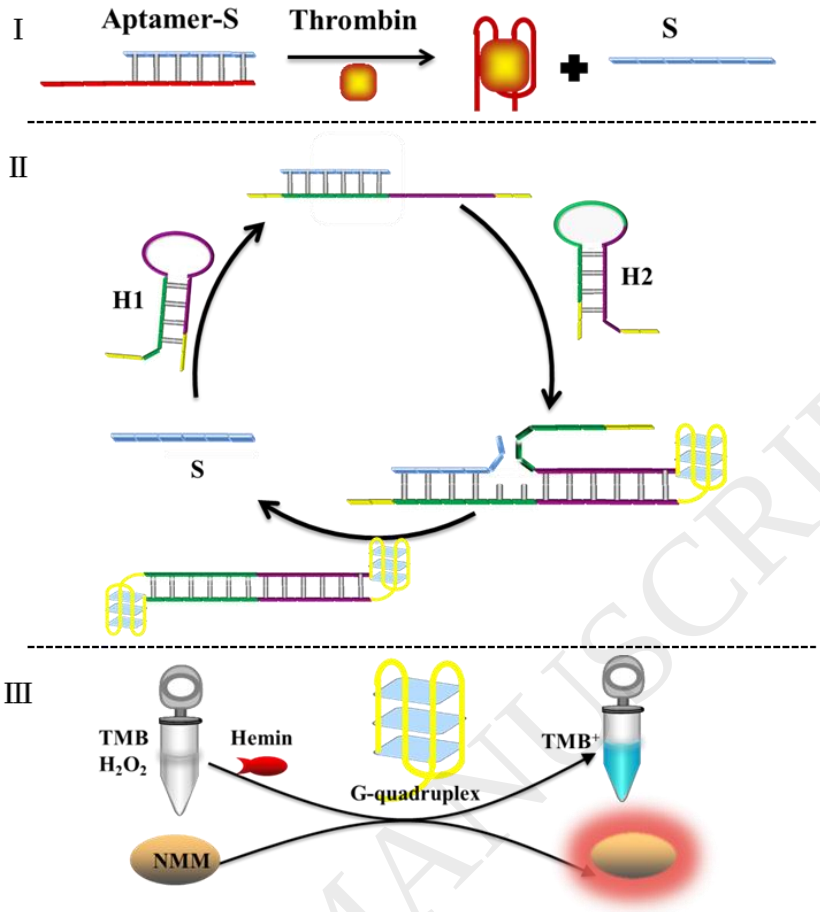

Taking the advantage of the high selectivity of aptamers and enzyme-free catalyzed hairpin assembly (CHA) amplification strategy, we herein describe a label-free and enzyme-free sensitive fluorescent and colorimetric strategy for amplified thrombin detection in this paper. To support both biological inquiry and technological innovation, thermodynamic models are introduced to predict the minimum energy secondary structure of interacting nucleic acid strands and calculate the partition function and equilibrium concentration for complexes in our system. Then, the thermodynamics properties of interacting DNA strands and the reactions of toehold strand displacement-driven assembly have been simulated, validating the feasibility of the theory and optimizing the follow-up lab tests. Following that, our strategy for thrombin detection is proved to be feasible and effective in biological experiments.

Highlights

- A model and algorithm has been introduced for analyzing the thermal performance of interacting DNA strands, demonstrating the validity of DNA sequences in our strategy.
- The reaction processes of catalytic hairpin assembly in this sensor are simulated to preliminary verify the theoretical feasibility prior to the test.
- The sensing model has good capability of thrombin detection with no fluorescent modification, making the detection method more facile, economical and effective.
- The reaction process is verified and optimized initially by simulations before attempting to build them in lab, to ensure that the actual experiments are more efficient and saves.
- Three experimental methods, fluorescent/colorimetric/PAGE, are used to verify the feasibility of the sensor.

Abstract

The development of efficient and convenient strategy without involving enzyme or complex nanomaterial for the micro molecules detection has profound meaning in the diagnosis of diseases. Herein, taking the advantages of the strong affinity of aptamer and catalyzed hairpin assembly, we develop a new non-label optical amplified strategy for thrombin detection in this work. To support both biological inquiry and technological innovation, thermodynamic models are introduced to predict the minimum energy secondary structure of interacting nucleic acid strands and calculate the partition function and equilibrium concentration for complexes in

our system. Then, the thermodynamics properties of interacting DNA strands and the reactions of toehold strand displacement-driven assembly have been simulated, validating the feasibility of the theory and optimizing the follow-up lab tests. Following that, our strategy for thrombin detection is proved to be feasible and effective in biological experiment. Taken together, such a biosensor has a good potential in bioactive molecules detection and disease diagnosis for future biological research.

Keyword: Computation and simulation; catalyzed hairpin assembly; fluorescence biosensor; DNA strand displacement; G-quadruplex

1. Introduction

Biosensor is actually a molecular sensor, which consists of a biomolecular recognition mechanism and a signal transduction technique [1]. This cost-effective and portable equipment is capable of carrying out rapid qualitative and quantitative analysis of analyte at decentralized locations. As a powerful detection and analysis tool, it have raised widespread concern in biomedical research, health care, environmental monitoring, and homeland security [2-3]. For example, ultrasensitive electrochemical biosensors based on nano-materials have been proposed for HIV gene detection in recently years [4-5]. The qualitative and quantitative analysis of bladder cancer is extremely significant in early stage of clinical diagnosis, so this protein is also used as a target of sensors for in-depth study [6]. However, developing more convenient and effective biosensor is still the main objective, and various signal

amplification techniques are being studied to improve sensitive at present [7-10].

Among them, catalytic hairpin assembly (CHA) is a common signal amplification method under isothermal and non-enzyme conditions, which is essentially DNA strand displacement reaction [11]. With the advantages of excellent information accumulation, high-performance parallel computing and flexible programmability, DNA strand displacement technology has been extensively studied in the fields of molecular computing, nano-machine, diagnosis and treatment of the diseases. In addition, the construction of the biosensor based on this displacement reaction is of great research significance by mastering the design procedures. Combining the predictability of Watson–Crick base pairing with the programmability of the DNA base sequence [12], researchers are able to build and manipulate molecular machines accurately to achieve multiple types of molecular calculations.

With these outstanding features, Visual DSD [13] has been proposed to aid the design of various systems implemented experimentally, as a tool for the design and analysis of strand displacement reaction. Support for reusable module in program code makes it easy and quick to build more complex system using pre-designed components. That means this tool can improve efficiency and productivity of DNA device design and analysis by carrying out simulates before laboratory testing, thereby saving materials and reducing time consuming [14-15].

The prediction of folded RNA/DNA structure has also considerable biological importance. Here, thermodynamic models are based on nucleic acid secondary

structure and nearest-neighbor identities [16] underlying dynamic programming algorithms. They have been used to predict the minimum energy secondary structure (MFE) [17] and compute the partition function over secondary structure set [18]. By rational DNA sequences design, synthetic nucleic acid sets can be programmed to self-assemble into complicated structural systems, which can be used to implement dynamic mechanical task [19]. The development of nucleic acid nanotechnology is extremely beneficial to many fields of science and technology, such as biocomputing, molecular robotics, and biosensing and so on.

In our work, a label-free optical sensing platform based on DNA strand displacement has been constructed and investigated, taking a pivotal biological functional protein-thrombin as example [20]. Before biological experiments, we introduce a model and algorithms firstly for analyzing the thermal performance of interacting DNA strands, demonstrating the validity of DNA sequences in our strategy. Next, to preliminary verify the theoretical feasibility, the reaction processes of catalytic hairpin assembly are simulated by Visual DSD prior to the test. At last, our strategy for thrombin detection has been validated to be feasible and effective by biological experiments. It is worth noting that the sensing performances such as sensitivity, specificity, real serum test and optimum experimental conditions, are tested and discussed in our another experiment [21].

2. Principle of the proposed method

Detection model design As shown in Fig. 1, the optical platform for thrombin

detection consists of three parts: (I) Target recognition process. At the beginning of the reaction, due to strongly binding with corresponding aptamer, thrombin binds to its aptamer strand and the S strand is released. (II) Signal amplification process. In essence, it is a toehold strand displacement-drive CHA reaction. More importantly, we ingeniously introduce two special hairpin structures of which partial stem can serve as the substrate of trigger chain, and quadruplex-rich sequences can form G-quadruplex. The S chain is used to trigger hairpins assembly, and then released to partake in next round of CHA reaction, generating a large number of ds-DNA (H1:H2) with G-quadruplexes at both ends. (III) Signal transformation and readout. There are many G-quadruplex structures in solution by previous signal amplification process. Fortunately, we have found that the special structure has many excellent chemical properties in biosensing for molecular detection. For example, there are a large number of fluorescent signals under the action of NMM (N-methyl-mesoporphyrin IX) [22-23]. Besides, the special G-rich oligomer can interact with hemin to produce peroxidase-mimicking DNAzymes and catalyze the oxidation reaction of H_2O_2 [24]. Under this action, TMB (3,3’,5,5’-tetramethylbenzidine) is oxidized from colorless to blue visible to the naked eye [25]. Briefly, in this process, the concentration signal of G-quadruplex is converted into a corresponding fluorescent or color variation that be observed by the naked eyes or instrument.

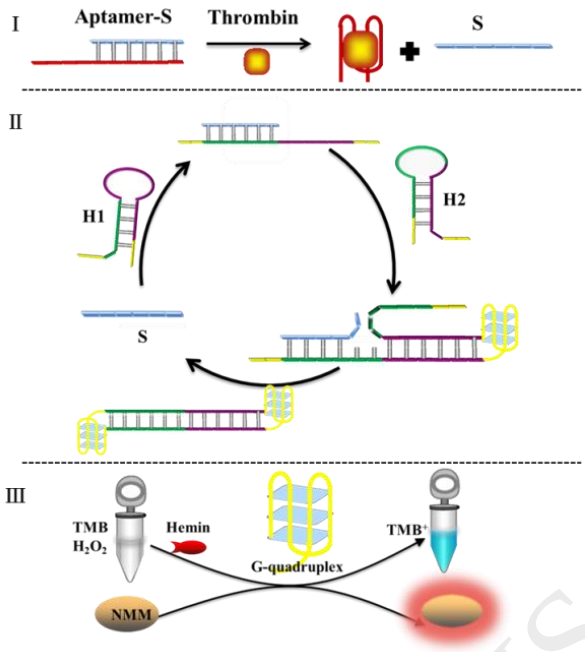

Fig. 1. Schematic diagram of biosensor for thrombin detection.

Sequence design and analysis According to the principle, we have designed four ss-DNA (Aptamer, S, H1, H2) in Table 1. These strands are obtained by NUPACK Design Module [18], and then modified slightly some modifications according to their biological characteristics.

Table 1 Sequences of oligonucleotides.

Name	Sequences
Aptamer	5'-GGT TGG TGT GGT TGG AAT AGT C-3'
S	5'-AGT CAC ACG GAC TAT TCC AA CC-3'
H1	5'-GGG TAA TAG TCC GTG TGA CTA TGG ACT ATA GGA GTC ACA CGG GCG GGT AGG G-3'
H2	5'-GGG TTG TAT GAC TCC TAT AGT CCA TAG TCA CAC GGA CTA TTG GGC GGG TAG GG-3'

Since secondary structures of nucleic acid are crucial for the DNA/RNA functionality, a prediction algorithm is presented to analyze and verify the thermal

characteristics of designed strands in ours work. In generally, thermodynamic model is used to predict MFE and compute the partition function. Then, the partition function is of great significance not only for researching the conformational ensemble, but also for evaluating the nucleic acid sequence in design.

More concretely, for a given DNA/RNA sequence, the base-pairing graph of its structure is decomposed into distinct loop configurations based on thermodynamic model (Figure 2A). The loop with different loop sequences, lengths and types corresponds to unequal enthalpic and entropic values [26]. To be specific, the free energy of secondary structure *s* is considered as a estimation according to the sum of the empirically determined free energies of the constituent loops in Eqs. (1). Then, partition function is a weighted sum over the set of all possible secondary structures Γ in in Eqs. (2), where *k* and *T* represent the Boltzmann constant and temperature.

$$\Delta G(s) = \sum_{\text{loop}\in s} \Delta G(\text{loop}) \qquad (1)$$

$$Q = \sum_{s\in\Gamma} e^{-\Delta G(s)/kT} \qquad (2)$$

Hence, the partition function for sequence of *N* length $\mathrm{Q} = \mathrm{Q}_{1\mathrm{N}}$ can be calculated with a dynamic programming algorithm of cubic order [27]. Based on these calculations, the MFE structure of hairpins H1 and H2 used in our design has been computed and simulated. The results show that their structures are consistent with design expectation and have lower free energy at 37℃ (ΔG(H1)=14.48 kcal/mol, ΔG(H2)=13.10 kcal/mol).

Then, the final equilibrium concentration of each complex in the thermodynamic

limit of large populations can be calculated. Consider the tube containing the set of strand species Ψ_0 that interact with each other to form the set of complex species Ψ. The first step is to calculate the partition function $Q(\phi_j)$ for each complex $j \in \Psi$, with sequence ϕ_j and structural ensemble Γ_j in Eqs. (3) [28].

$$Q(\phi_j) = \sum_{s \in \Gamma_j} e^{-\Delta G(\phi_j, s)/kT} \quad (3)$$

The partition function is then a weighted sum over the set of all secondary structure $s \in \Gamma_j$ in Eqs. (4). Here, *k* and *T* are same with above.s

$$p(\phi_j, s) = \frac{e^{-\Delta G(\phi_j, s)/kT}}{Q(\phi_j)} \quad (4)$$

Next, the base-pairing probability matrix $P(\phi_j)$ is described for the equilibrium base-pairing properties of complex *j* in Eqs. (5).

$$P^{a,b}(\phi_j) = \sum_{s \in \Gamma_j} p(\phi_j, s) S^{a,b}(s) \quad (5)$$

Here, base pair a,b froms at equilibrium within ensemble Γ_j and *S*(*s*) is the structure matrix. In this, $S^{a,b}(s)$ is 1 when structure s contains base pair a,b, otherwise it is 0.

Let $Q_\Psi \equiv Q_j, \forall j \in \Psi$ denotes the set of complex partition function. The equilibrium concentration of complexes, x_Ψ, is determined by solving the optimal problems in Eqs. (6) [29].

$$\min_{x_\Psi} \sum_{j \epsilon \Psi} x_j (\log x_j - \log Q_i - 1) \quad (6)$$

$$\text{subject to} \quad A_{i,j} x_j = x_i^0 \quad \forall i \in \Psi^0$$

Here, the constraints subject to conservation of mass. A represents the stoichiometry

matrix with entries $A_{i,j}$ corresponding to chains number of type i in complex j, and x_i^0 represents the total concentration of strand i.

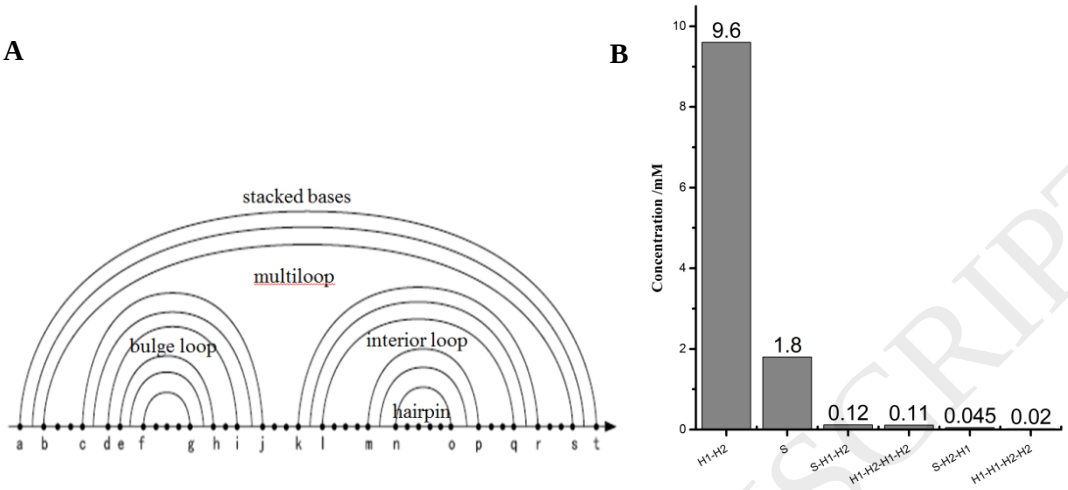

Fig. 2. (A) Canonical loops of nucleic acid secondary structure. (B) Simulation results of the CHA process in our strategy.

According to the calculation introduced above, Fig. 2B shows the equilibrium concentrations for every species of mixing solution in CHA reaction. In equilibrium, there are multiple nucleic acid structures in the solution. The proportion of H1–H2 strands is up to 96%, which consistent with our expectations. At the same time, background products produced by additional reactions, such as S–H1–H2, H2–H1–H2–H1, can be neglected to some extent. Therefore, the rationality of the sequence design of designed hairpins can be proved by simulations in theory.

3. Results and discussion

Reaction mechanism Consider the DNA reaction diagram [30] of biosensors for thrombin detection given in Fig. 3. Here, the strands inside the bold boxes are initial reactants. The strands at the end of the gray line with arrows represent the products of positive reaction while those at the end of the black arrow represent the products of

the negative reaction. The number of each reaction in this diagram stands for DNA bind and unbind rate. For convenience, we regard the *thrombin* as ss-DNA complementary to its aptamer.

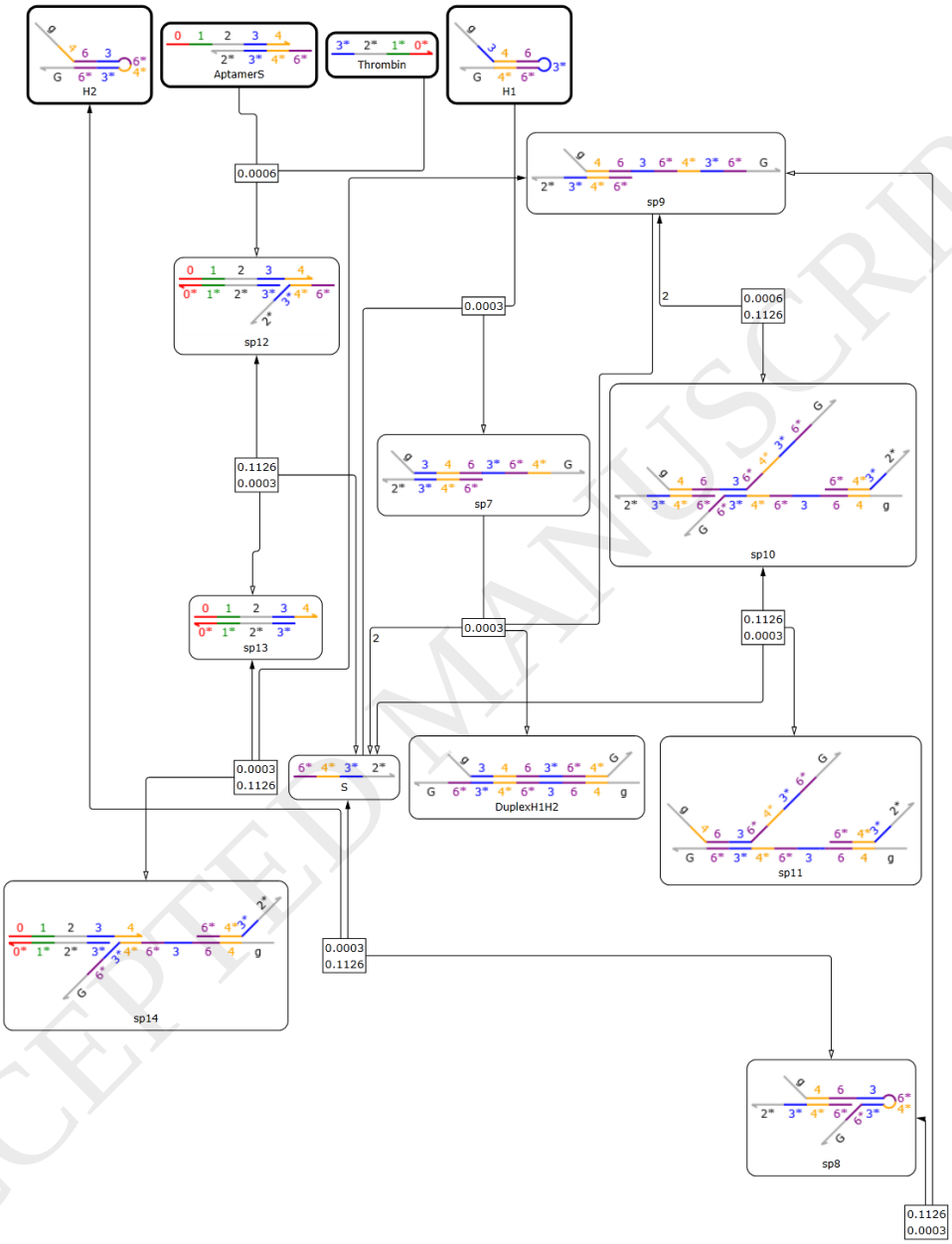

Fig. 3. DNA reaction diagrams of the DNA strand displacement in our design.

According to our design, the <g>, <G> domains are quadruplex-forming structure together and the <0>, <3>, <4> domains are the toehold. Other represents the branch migration domains. Ideally, *Thrombin* will bind to *AstamerS* to produce *sp13* and

liberated *S*. Then, due to the toehold domain <3*> of *S* hybridizing with exposed complement toehold domain <3> of *H1*, the hairpin of *H1* can be unfolded and forms *sp7* with strand displacement reaction. Subsequently, *sp7* exposed toehold domain <4*> binds spontaneously to toehold domain <4> of *H2*. Owing to branch migration from 5' to 3', the strand of *S* is displaced and dsDNA *DuplexH1H2* appears. Next, *S* participates in the multiple round of CHA with H1 and H2 successively, resulting in the generation of massive *DuplexH1H2*.

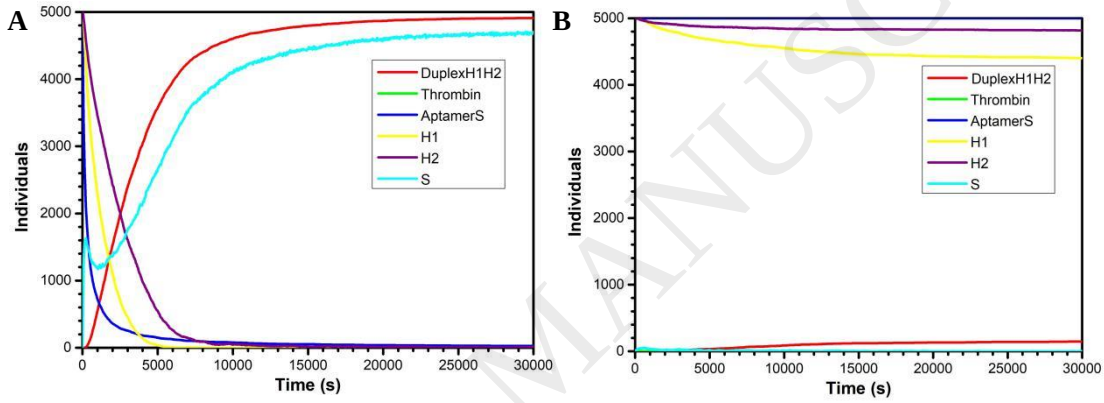

Fig. 4. Visual DSD simulations. The change in the number of strands over time in the system with thrombin (A); without thrombin (B).

Finally, quantitative changes in strands over time under different circumstances can be seen in Fig. 4. When thrombin exits, the amount of *thrombin* and the *AptamerS* strands is rapidly reduced to 0 because of the interaction between them (Fig. 4A, green, blue line). The free *S* strands first rise, then fall, to patriciate in hairpins assembly, and rise to maximum eventually (Fig. 4A, light blue line). In CHA reaction, the number of *H1* and *H2* reduces quickly to minimum due to self-assembly reaction (Fig. 4A, yellow, purple line), while the reaction product-*DuplexH1H2* raise rapidly to the maximum and maintained balance ultimately (Fig. 4A, red line). In contrast, Fig. 4B is shown as a control group experiment without target *thrombin*. Both *thrombin*

and *S* are almost unchanged at 0 (Fig. 4B, green, light blue line), so the *AptamerS* also maintains in the initial state (Fig. 4B, blue line). However, traces of *DuplexH1H2* still appeared in the solution due to the weak interaction (Fig. 4B, yellow, purple, red line, respectively). In summary, the value of DuplexH1H2 in the presence of thrombin is amost 30 times more than that in the absence of thrombin. Accordingly, it proves the feasibility of the sensing model in theory by simulating the experiment process.

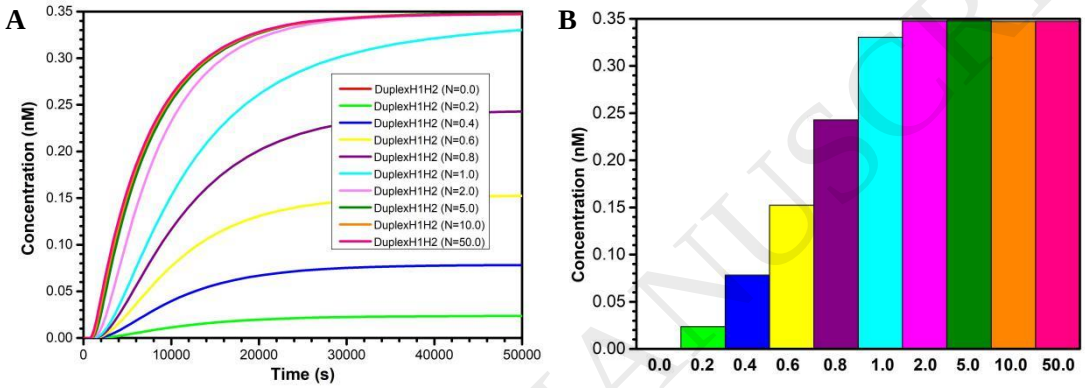

Fig. 5. Visual DSD simulations (A) The DuplexH1H2 strand's change over time in the system with different thrombin concentrations (B) The concentration of DuplexH1H2 strands at the equilibrium state corresponding to different thrombin concentrations, respectively.

Optimization of the reaction conditions To evaluate target recognition process of the present strategy, different concentrations of thrombin are measured under the condition of standardization. Fig. 5A shows the change of DuplexH1H2 strands over time in cases where the thrombin concentration is 0, 0.2, 0.4, 0.6, 0.8, 1.0, 2.0, 5.0, 10.0, and 50.0 nM, respectively. It can be seen that the reaction rate gradually increases along with the increase of thrombin concentration in the range from 0.2 to 2.0 nM. At the equilibrium state, the amount of DuplexH1H2 strands corresponding different thrombin concentrations can be seen from Fig. 5B. Obviously, when the thrombin concentration is greater than 1 nM, the number of products reaches the

maximum value. From the simulation experiment, 2 nM can be selected as the optimal thrombin concentration at the beginning of biological experiments due to the faster convergence and higher product conversion rates.

Next, to achieve the optimal amplification performance, the toehold length of first hairpin H1, the incubation temperature of CHA, the concentration of hairpins H1 and H2 are optimized. Firstly of all, toehold-mediated strand displacement reaction (TSDR) is a common reaction pattern in vivo. By adjusting the number of bases and the sequence composition of toehold, TSDR rate control can be achieved and further influent the next reaction process. When the toehold length is too short, the H1 will unable to fully hybridize with trigger S. However, too long toehold length will lead to the irreversible binding between S and H1, which is conducive to hairpin self-assembly and next CHA circulation. Six kinds of H1 strands with different length of toeholds (3, 4, 5, 6, 7, 8 nt) are simulated in Fig.6A. We can see that 6nt toeholds length lead to the best of product yield (H1:H2) and is chosen for the following experiments. In addition, temperature affects not only the stability of the hairpins structure, but also the bind, unbinding and migration rate of strand displacement reaction. Hence, the incubation temperature of CHA is also simulated in Fig. 6B. In the absence of trigger S, only slight change can be achieved (Fig. 6B, black line). Upon the addition of S, the product yield increases rapidly with the increase of the incubation temperature, and then reaches equilibrium at 35℃ (Fig. 6B red line). Therefore, 35℃ is determined to be the appropriate temperature initially in actual biological tests.

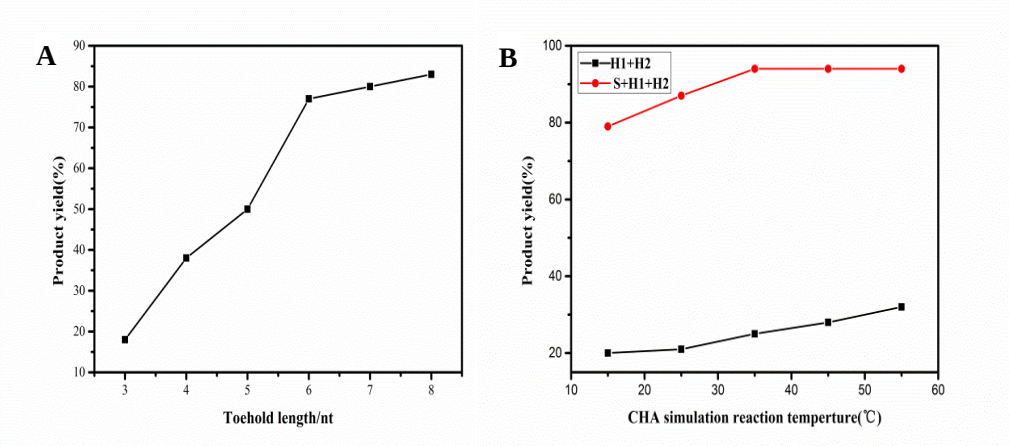

Fig. 6. Simulation results: Optimization of experimental conditions. (A) Toehold length of H1. (B) Incubation temperature of CHA.

In addition, many reactions under different conditions are simulated to roughly determine the concentration range of each DNA chains. The amount of hairpins structure H1, H2 involved in self-assembly also greatly influences the reaction process and results. According to Fig. 7, we can see the change of DuplexH1H2 strands over time in cases where the concentration ratio of hairpin to substrate AptamerS is 1, 2, 3, 4, 5, 6, 7, 8, and 9, respectively. Simulation result shows that the reactions reach saturation basically and the conversion rate tends to be the same, when the ratio is greater than 5. Considering the discussed above and economic considerations, experimental results are expected to be best when the amount of hairpin structure H1, H2 is about 5-6 times of the substrate AptamerS.

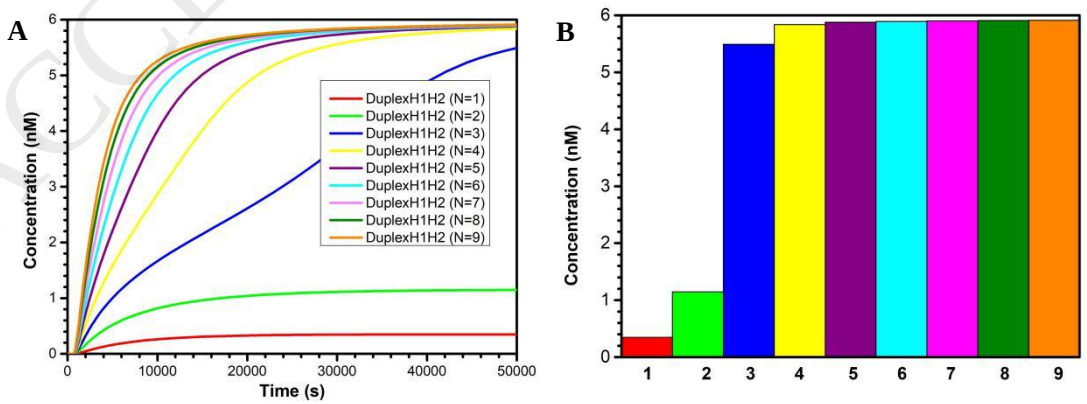

Fig. 7. Visual DSD simulations (A) The change in the number of DuplexH1H2 strands over time in the system in cases where the concentration ratio of hairpin to substrate AptamerS is 1, 2, 3, 4, 5,

6, 7, 8, and 9, respectively. (B) The concentration of DuplexH1H2 strands at the equilibrium state corresponding to the above conditions, respectively.

Feasibility for thrombin detection in biological experiments This dynamic process molecular reaction is validated by 10% native-PAGE (polyacrylamide gel electrophoresis) in Fig. 8A. From this result, we can observe several distinct bands for Aptamer-S (lane 1), H1 (lane 2) and H2 (lane 3), respectively. The mixture of two hairpins had the same bands as H1 or H2 (lane 4). It indicates that the H1 and H2 can coexist and almost no self-assembly reaction without trigger strands. Then, there is a blurred band above H1 and H2 with the addition of Aptamer-S, because two hairpins are likely to generate slight amounts of H1/H2 complex (lane 5). Next in the presence of thrombin, a distinct band corresponding to H1/H2 ds-DNA appears in mixed solution (lane 6). Besides, the band intensities of H1, H2 and Aptamer-S became weaker than those in lane 5. This bands distribution shows that thrombin liberates S from the Aptamer-S duplex, then the released S effectively triggers the catalytic hairpin assembly to produce numerous H1/H2 complex with the consumption of H1 and H2. Therefore, the native-PAGE experiments in accordance with simulation, give more sufficient verification of this proposed biosensor.

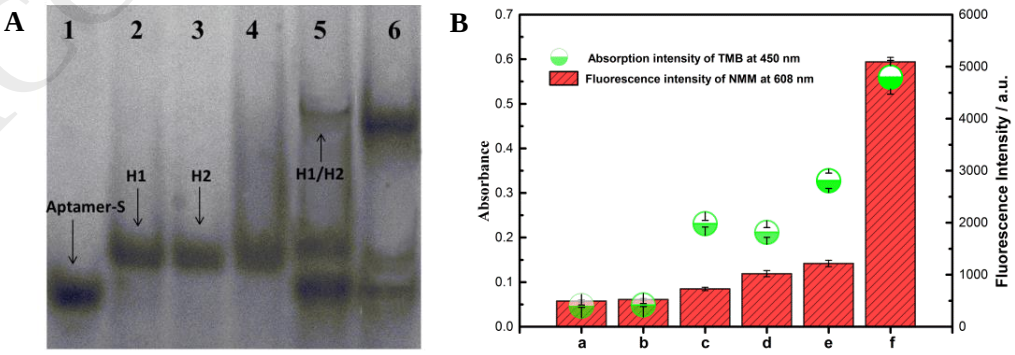

Fig. 8. (A) 10% native-PAGE analysis of different solutions: (1) Aptamer-S; (2) H1; (3) H2; (4) H1and H2; (5) Aptamer-S, H1 and H2; (6) Aptamer-S, H1, H2 and thrombin. The concentration of

thrombin, Aptamer-S, H1, and H2 are 1 nM, 5 nM, 5 nM, and 5 nM, respectively. (B) Absorption/ fluorescence intensity value of different samples. Sample a-f correspond to 1-6, respectively.. The concentration of thrombin, Aptamer-S, H1 and H2 are 1 nM, 50 nM, 300 nM and 300 nM, respectively. Error bars=3.

Meanwhile, two kinds of optical detection methods are also performed to prove the feasibility of this design. On the one hand, the fluorescent intensity values (at 608 nm) of different samples are measured after incubation with NMM for 25 min. As shown in Fig. 8B, negligible fluorescence signal is obtained from sample containing Aptamer-S (sample b). Compared to it, there is only a slight increase in the case of thrombin addition (sample c). This is a result of that the aptamer strands fold into G-quadruplex, leading to the slightly enhanced fluorescence signal from NMM. In addition, the mixtures of hairpins (sample d) and the mixtures of Aptamer-S, H1, H2 (sample e) retain the low fluorescence intensity, and increase slightly compared to the former three sample, which may be due to the weak interaction between H1 and H2 forming a few G-quadruplex. Next, thrombin is added to the mixture solution with Aptamer-S, H1, H2 probes, and causes significant fluorescence enhancement from NMM (sample f). The results demonstrate that thrombin effectively liberates S strands from the Aptamer-S duplex, which triggers the assembly of H1 and H2. Thereby, a large number of generated G-quadruplexes lead to a significantly amplified fluorescence response from NMM. On the other hand, the NMM was replaced by TMB, producing a visible green color. According to the same strategy, the presence of thrombin would trigger the amplification reaction. As shown in Fig. 6A, the sample e can offer the highest colorimetric signal, which not only measured by spectrophotometer, but also clearly distinguished by the naked eyes.

4. Conclusion

In conclusion, we have developed an enzyme-free and label-free optical biosensor for thrombin detection based on target-induced assembly, verified by simulations and biological tests. The follows are several excellent merits in our designed sensing. First of all, this strategy allows a homogeneous assay of thrombin activity without fluorescent labels, making it much more convenient and cost-effective. In addition, simulation experiments can not only verify the reaction process, but also preliminarily optimize the reaction conditions, so as to complete actual biological experiments more efficiently in lab. Next, this fluorescent approach does not require constrained proteinase and complicated thermal-cycling procedure for signal amplification. There is low detection limit with pM level, which has been verified by our previous experiments [21]. Finally, it has the potential to be easily extended for other analyte detection by ingeniously designing molecular probe. Taken together, this method has good prospect in interdisciplinary subject of computer and biology, which exhibits enormous application potentiality in clinical diagnosis of genetic diseases.

Acknowledgements

This research was funded by National Natural Science Foundation of China (Grant No. 61572302, No. 61272246).

References

1. Fan, X., White, I.M., Shopova, S.I., Zhu, H., Suter, J.D., Sun, Y.: Sensitive optical bi osensors for unlabeled targets: a review. Analytica Chimica Acta **620**(1), 8-26 (2008)

2. Nguyen, V.T., Kwon, Y.S., Gu, M.B.: Aptamer-based environmental biosensors for sm all molecule contaminants. Current Opinion in Biotechnology **45**, 15-23(2017)

3. Tan, Y., Guo, Q., Zhao, X., Yang, X., Wang, K., Huang, J., Zhou, Y.: Proximity-depe ndent protein detection based on enzyme-assisted fluorescence signal amplification. Bio sensors & Bioelectronics **51**(3), 255-260 (2014)

4. Wang, Y., Bai X., Wen, W., Zhang, X., Wang, S.: Ultrasensitive electrochemical biose nsor for HIV gene detection based on graphene stabilized gold nanoclusters with exon uclease amplification. ACS Applied Materials & Interfaces **7**(33), 18872-18879 (2015)

5. Hu, Y., Li, H., Li, J.: A novel electrochemical biosensor for HIV-related DNA detecti on based on toehold strand displacement reaction and cruciform DNA crystal. Journal of Electroanalytical Chemistry **822**, 66-72 (2018)

6. Kollarik, B., Zvarik, M., Bujdak, P., Weibl, P., Rybar, L., Sikurova, L.: Urinary fluore scence analysis in diagnosis of bladder cancer. Neoplasma **65**(2), 234-241 (2018)

7. Kong, L., Xu, J., Xu, Y., Xiang, Y., Yuan, R., Chai, Y.: A universal and label-free a ptasensor for fluorescent detection of atp and thrombin based on sybr green i dye. Bi osensors & Bioelectronics **42**(1), 193-7 (2013)

8. Zheng, A.X., Wang, J.R., Li, J., Song, X.R., Chen, G.N., Yang, H.H.: Enzyme-free fl uorescence aptasensor for amplification detection of human thrombin via target-catalyz ed hairpin assembly. Biosensors & Bioelectronics **36**(1), 217-221 (2012)

9. Niu, S., Qu, L., Zhang, Q., Lin, J.: Fluorescence detection of thrombin using autocata lytic strand displacement cycle reaction and a dual-aptamer dna sandwich assay. Analy tical Chemistry **421**(2), 362 (2012)

10. Yin, P., Choi, H.M.T., Calvert, C.R., Pierce, N.A.: Programming biomolecular self-asse mbly pathways. Nature **451**(7176), 318-322 (2008)

11. Li, J., Macdonald, J.: Advances in isothermal amplification: novel strategies inspired b y biological processes. Biosensors & Bioelectronics **64**(64C), 196-211 (2015)

12. Fu, B., Cao, J., Jiang, W., Wang, L.: A novel enzyme-free and label-free fluorescence aptasensor for amplified detection of adenosine. Biosensors & Bioelectronics **44**(11), 52-56 (2013)

13. Lakin, M.R., Youssef, S., Polo, F., Emmott, S., Phillips, A.: Visual dsd: a design and analysis tool for dnastrand displacement systems. Bioinformatics **27**(22), 3211-3213 (2011)

14. Dhanaraj, P., Devadas, A., Muthiah, I.: A comparative meta-genomic analysis of hpv s

trains: A step towards the design, synthesis and characterization of noval quenazoline derivative for antiviral activity. Computational Biology & Chemistry **73**, 213-220 (2018)

15. S, M., A, S.-Y., A, M., A, M.-N.: Computational structure analysis of biomacromolecule complexes by interface geometry. Computational Biology & Chemistry **47**(6), 16-23 (2013)
16. Tinoco, I., Uhlenbeck, O.C., Levine, M.D.: Estimation of secondary structure in ribonucleic acids. Nature **230**(5293), 362-367 (1971)
17. Waterman, M.S.: Secondary structure of single-stranded nucleic acidst **1**, 167-212 (1978)
18. Dirks, R.M., Pierce, N.A.: An algorithm for computing nucleic acid base-pairing probabilities including pseudoknots. Journal of Computational Chemistry **25**(10), 1295-304 (2004)
19. Dirks, R.M., Bois, J.S., Schaeffer, J.M., Winfree, E., Pierce, N.A.: Thermodynamic analysis of interacting nucleic acid strands. Siam Review **49**(1), 65-88 (2007)
20. Zhu, H., Suter, J.D., White, I.M., Fan, X.: Aptamer based microsphere biosensor for thrombin detection.Sensors **6**(8), 785-795 (2006)
21. Zhang, Y., Wang, L., Wang, Y., Dong, Y.: A non-label and enzyme-free sensitive detection method for thrombin based on simulation-assisted dna assembly. Sensors **18**(7), 2179 (2018)
22. Li, H., Ren, J., Liu, Y., Wang, E.: Application of dna machine in amplified dna detection. Chemical Communications **50**(6), 704-706 (2013)
23. Wang, K., Ren, J., Fan, D., Liu, Y., Wang, E.: Integration of graphene oxide and dna as a universal platform for multiple arithmetic logic units. Chemical Communications **50**(92), 14390-14393 (2014)
24. Li, J., Jia, Y., Zheng, J., Zhong, W., Shen, G., Yang, R., Tan, W.: Aptamer degradation inhibition combined with dnazyme cascade-based signal amplification for colorimetric detection of proteins. Chemical Communications **49**(55), 6137-6139 (2013)
25. Li, W., Liu, Z., Lin, H., Nie, Z., Chen, J., Xu, X., Yao, S.: Label-free colorimetric assay for methyltransferase activity based on a novel methylation-responsive dnazyme strategy. Analytical Chemistry **82**(5), 1935-41 (2010)
26. Dirks, R.M., Pierce, N.A.: A partition function algorithm for nucleic acid secondary structure including pseudoknots - dirks - 2003 - journal of computational chemistry wiley online library. Journal of Computational Chemistry **24**(13), 1664-77 (2010)
27. Mccaskill, J.S.: The equilibrium partition function and base pair binding probabilities for rna secondary structure. Biopolymers **29**(6-7), 1105-1119 (2010)
28. Wolfe, B.R., Pierce, N.A.: Sequence design for a test tube of interacting nucleic acid

strands. Acs Synthetic Biology **4**(10), 1086 (2014)

29. Gallian, J.A.: Contemporary abstract algebra. 2nd edition. Cengage Learning Emea **24** (13), 2309-2316 (1998)

30. George, A.K., Singh, H.: Dna implementation of fuzzy inference engine: Towards dna decision-making systems. IEEE Transactions on Nanobioscience **PP**(99), 1-1 (2017)